Journal of Power Sources 395 (2018) 369–378

Contents lists available at ScienceDirect

Journal of Power Sources

journal homepage: www.elsevier.com/locate/jpowsour

Methodology to determine the heat capacity of lithium-ion cells

Thomas S. Bryden[a,*], Borislav Dimitrov[a], George Hilton[a], Carlos Ponce de León[a], Peter Bugryniec[b], Solomon Brown[b], Denis Cumming[b], Andrew Cruden[a]

[a] Faculty of Engineering and the Environment, University of Southampton, Southampton, SO14 1BJ, United Kingdom
[b] Department of Chemical and Biological Engineering, University of Sheffield, Sheffield, S1 3JD, United Kingdom

HIGHLIGHTS

- New method to determine the specific heat capacity of lithium-ion cells.
- Same method is applicable to cylindrical, pouch and prismatic cells.
- Results verified using calorimetry.
- Method uses common, inexpensive equipment found in many laboratories.
- Thermal model results validated experimentally for a range of operating conditions.

GRAPHICAL ABSTRACT

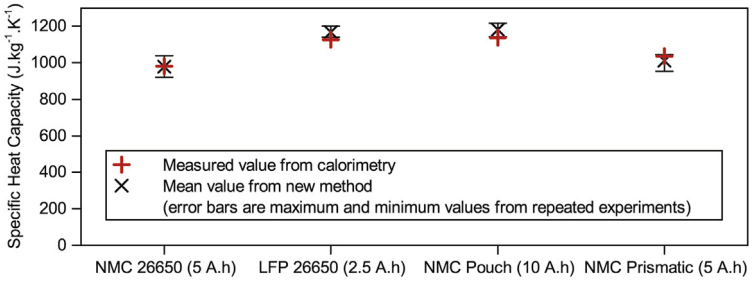

ARTICLE INFO

Keywords:
Thermal modelling
Specific heat capacity
Lithium-ion battery

ABSTRACT

In this paper a novel method to determine the specific heat capacity of lithium-ion cells is proposed. The specific heat capacity is an important parameter for the thermal modelling of lithium-ion batteries and is not generally stated on cell datasheets or available from cell manufacturers. To determine the specific heat capacity can require the use of an expensive (> £100 k) calorimeter or the deconstruction of the cell whereas the method proposed by the authors in this paper uses common equipment found in most battery laboratories. The method is shown to work for cylindrical, prismatic and pouch cells, with capacities between 2.5 Ah and 10 Ah. The results are validated by determining the specific heat capacity of the cells with use of a calorimeter and a maximum error of 3.9% found. Thermal modelling of batteries is important to ensure cell temperatures are kept within specified limits. This is especially true at rates over 1C, such as the fast charging of electric vehicles, where more heat is generated than lower rate applications. The paper ends by demonstrating how the thermal model that underpins the authors' methodology can be used to model the surface temperature of the cells at C-rates greater than 1C.

1. Introduction

Energy storage is a topic that has gained much research attention in recent years, primarily with the end goal applications in either the transportation or electricity grid support sectors. Lithium-ion batteries have emerged as the dominant energy storage technology for transportation applications and are also used for many grid support applications. Operating lithium-ion batteries within a limited temperature range, usually between 15 °C and 35 °C, is important for extending the lifetime of battery [1]. Operating outside the specified temperature range will reduce the lifetime of the battery and, in addition, if the battery becomes too hot and the temperature exceeds the

* Corresponding author.
E-mail addresses: t.s.bryden@soton.ac.uk (T.S. Bryden), b.h.dimitrov@soton.ac.uk (B. Dimitrov), g.hilton@soton.ac.uk (G. Hilton), c.a.ponce-de-leon-albarran@soton.ac.uk (C. Ponce de León), pbugryniec1@sheffield.ac.uk (P. Bugryniec), s.f.brown@sheffield.ac.uk (S. Brown), d.cumming@sheffield.ac.uk (D. Cumming), a.j.cruden@soton.ac.uk (A. Cruden).

https://doi.org/10.1016/j.jpowsour.2018.05.084
Received 20 April 2018; Accepted 27 May 2018
0378-7753/ © 2018 Elsevier B.V. All rights reserved.

thermal runaway onset temperature, thermal runaway can occur leading to catastrophic failure [2]. Thermal modelling of lithium-ion batteries is therefore required during the battery design process to ensure the battery is designed to operate safely within the specified limits.

The thermal modelling of lithium-ion batteries becomes essential when batteries are operated at high rates where more heat is generated. Electric vehicle batteries may be required to operate at rates above 1C continuously while charging. The aim to increase charging rates in the future means thermal modelling and thermal management of the batteries will become even more important [3]. Hybrid and plug in hybrid electric vehicles have smaller capacity batteries than electric vehicles, however the cells have to operate at much higher rates and so thermal modelling is also important. An example are the Blue Energy cells, which are installed in many hybrid vehicles, these cells have a capacity of 5 Ah but may have to operate at up to 300 A for short periods during regenerative braking [4].

Thermal models of lithium-ion cells often start with a simple heat balance at a single point [5]. The rate heat is released or absorbed at the point is equal to the rate heat is generated or consumed at the point plus the rate heat is transferred to or from the point, this is described in more detail in Section 2. One and two dimensional models of lithium-ion cells that use few points can be created by programming the finite difference calculations [6]. More detailed three dimensional models using many points may require finite element modelling to predict the temperature in more complicated scenarios [7–10].

Differences between thermal models of lithium-ion cells arise due to the complexity of the cell geometry and the details of the different materials used in the cell, including their exact locations within the cell and the types of heat generation and consumption considered, this is described in more detail below. As with all modelling a trade off between accuracy and complexity must be considered.

The specific heat capacity of the cells is a critical thermal parameter that is required for all cell thermal models, irrespective of the thermal model employed. The heat capacity of an object is a measure of how easy it is to change the temperature of the object by transfer of heat. Depending on the required model complexity there may be one value for the heat capacity of the entire cell or multiple values at different locations within the cell [11–13], representing the different materials that the cell is constructed from. It should be noted that the specific heat capacity is not stated on cell datasheets and manufacturers often do not have data on the specific heat capacity of their cells. This paper focuses on modelling cases where a single value for the heat capacity is used.

One common method to find the heat capacity involves a weighted sum of the heat capacities of the materials inside the cell [14] however this either requires deconstructing the cell and determining the materials chemically or having detailed information regarding the make up of the cell, which normally is not available. A second common method is to use calorimetry [15], however the equipment to perform this calorimetry is expensive, often costing more than £100,000 and not commonly available in many laboratories. In this paper we demonstrate a novel method to determine the specific heat capacity of cells using common equipment found in most battery laboratories, the method requires only a battery analyser, temperature sensors and a fan.

As well as the specific heat capacity of a cell, a second parameter required for many thermal models is the thermal conductivity of the cells [16]. The thermal conductivity of the cell is a measure of how easily heat is transferred through the cell by conduction. The thermal conductivity varies within a cell depending on the direction of heat transfer [17]. Take for example a spirally wound cylindrical cell, the thermal conductivity will be different longitudinally and radially. Longitudinally, the heat is travelling through the same material, for example along a copper current collector. Radially, the heat is travelling through many layers of different materials, for example through the current collector, electrode, separator, etc. As an approximation, the model used in this paper does not differentiate between directions and uses a single value for the internal thermal resistance.

In the single point heat balance mentioned above, the rate at which heat is released or absorbed at a point and the heat transfer to and from a point are standard equations for thermal models, while the rate heat is generated or consumed in the cell is particular to lithium-ion battery thermal models. The estimation of the heat generation and consumption in a cell again depends on the model complexity and often four different terms of heat generation and consumption are discussed [18]: ohmic heating; reversible entropic heat; heat produced or consumed by any chemical reaction; heat of mixing.

In many thermal models of lithium-ion cells only the ohmic heating and reversible entropic heat terms are considered as they have the largest impact on temperature [19,20]. The ohmic heating term is the heat generated as current passes through the cell and is always generating heat when the current exists, it is equal to the current squared multiplied by the resistance. The entropic heat term is the entropy change of the cell reaction and it can either generate or consume heat, it is equal to the current multiplied by the temperature multiplied by the rate of change in open circuit voltage of the cell with temperature, which varies depending on the cell state of charge. The entropic heat term therefore requires significant cell characterisation of the open circuit voltage versus temperature across the range of state of charge which is a time consuming task [21]. Depending on the current rate of charge or discharge of the cell, either the ohmic heating term or the reversible entropic heat term may dominate, however note that the ohmic heating term is proportional to the current squared while the entropic heat term is only directly proportional to current.

This paper is structured as follows. The theory and description of the thermal model used by the authors is described in Section 2 and the experimental setup required for determining the specific heat capacity is described in Section 3. The novel method to determine the specific heat capacity of the cells is then described in Section 4. Section 5 presents the standard method to determine the specific heat capacity using a calorimeter and Section 6 compares the specific heat capacity values from Sections 4 and 5 for two cylindrical cells, one pouch cell and one prismatic cell. Section 7 discusses how the model can be used to predict the surface temperature of the cells during cycling with further discussion of surface temperature variations in Section 8. The paper conclusions are presented in Section 9.

2. Description of the cell thermal model

The lithium-ion cell thermal model used has previously been reported for a lithium-ion iron phosphate cell [22]. In this model heat is generated at a point inside the cell where this point has a specific heat capacity and a mass. The heat is then transferred from the inside of the cell to the cell surface where there is no mass or specific heat capacity. Finally, the heat is transferred from cell surface to the ambient environment as shown in Fig. 1. The internal and external heat transfer

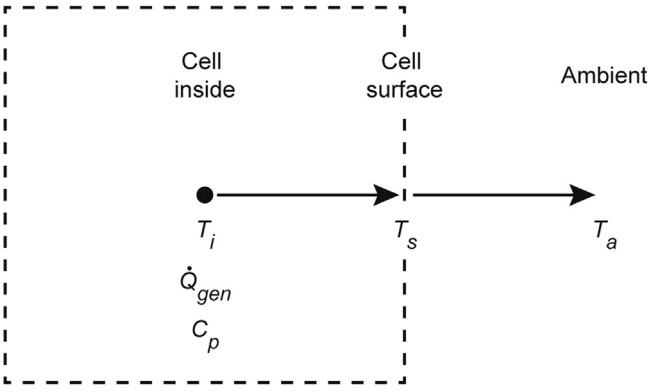

Fig. 1. Overview of cell thermal model.

coefficients include all heat transfer modes, namely conduction, convection and radiation. If heat is consumed within the cell or the ambient temperature is higher than the cell temperature then the heat will flow in the opposite direction to that illustrated in Fig. 1.

Conducting a heat balance at the point on the cell inside, the rate that heat is transferred to this point is equal to the rate at which heat is generated at this point ($\dot{Q}_{gen}$ (W)) minus the rate heat flows away from this point, as stated in Equation (1). The rate that heat is transferred to the point is related to the heat capacity (C_p $(J\ K^{-1})$ and the rate of internal temperature (T_i (K)) change with time (t (s)), as per the equation on the left hand side of Equation (1). The rate heat flows away from this point is related to the internal heat transfer coefficient (h_{in} $(W\ m^{-2}\ K^{-1})$), the internal area (A_{in} (m^2)) and the temperature difference between the internal temperature and the cell surface temperature (T_s (K)), as per the terms on the far right hand side of Equation (1). Throughout the experiments the internal area for each cell does not change and so the product of $h_{in}A_{in}$ is constant, and hence to use standard terms this product is normally stated as the inverse of the internal thermal resistance (R_{in} $(K\ W^{-1})$).

$$C_p\frac{dT_i}{dt} = \dot{Q}_{gen} - \frac{1}{R_{in}}(T_i - T_s) \tag{1}$$

Measuring the internal temperature of a cell is not possible with basic laboratory equipment as to place a thermocouple inside the cell to determinate internal temperature would require a glove box to provide an inert atmosphere in which the cell can be modified without internal cell components reacting with oxygen and or water. To eliminate the internal cell temperature from Equation (1), an energy balance at the cell surface is conducted. It is assumed that the cell surface point has no mass and no heat is generated at the cell surface point, therefore the rate heat flows to this point is equal to the rate heat flows away from this point as stated in Equation (2) and shown in Fig. 1. The rate heat flows away from this point is related to the external heat transfer coefficient (h_{out} $(W\ m^{-2}\ K^{-1})$), the external area (A_{out} (m^2)) and the temperature difference between the cell surface temperature and the ambient temperature (T_a (K)), as per the equation on the right hand side of Equation (2). Similar to above, the singular heat transfer term accounts for all modes of heat transfer and the external area will not change so the product of $h_{out}A_{out}$ is exchanged for the inverse of the external thermal resistance (R_{out} $(K\ W^{-1})$).

$$\frac{1}{R_{in}}(T_i - T_s) = \frac{1}{R_{out}}(T_s - T_a) \tag{2}$$

By solving Equation (2) for T_i, and assuming the ambient temperature is constant, substituting T_i into Equation (1) gives Equation (3).

$$C_p(R_{in} + R_{out})\frac{dT_s}{dt} = \dot{Q}_{gen}R_{out} + T_a - T_s \tag{3}$$

There are therefore four unknowns in Equation (3), $\dot{Q}_{gen}$ the heat generated inside the cell described below, C_p the heat capacity, R_{in} the internal heat transfer coefficient and R_{out} the external heat transfer coefficient. The output to the model is the surface temperature, which is found by rearranging Equation (3) to the form of Equation (4) and using a time step (Δt (s)), i.e. using an explicit Euler to discretise the ordinary differential equation.

$$T_s(t) = \frac{\dot{Q}_{gen}(t)R_{out} + T_a - T_s(t)}{C_p(R_{in} + R_{out})}\Delta t + T_s(t-1) \tag{4}$$

The heat generated or consumed inside a cell during charging and discharging has been investigated in detail in previous studies, as described in Section 1. The method used in this paper to determine the specific heat capacity involves charging and discharging the cells at the manufacturers quoted maximum charge and discharge rates and, subsequently in Section 7.2, the authors' cell thermal model is demonstrated at rates only over 1C. At these high rates (> 1C) the ohmic heating term is dominant as the ohmic heating is proportional to the current squared. Other studies found that including the entropic term produced only a small reduction of the maximum temperature error from 2.3 °C to 1.8 °C [22], and so it is not considered in this study. The ohmic heating is equal to the absolute value of the voltage of the cell (V (V)) minus the open circuit voltage at the cell state of charge ($V_{OCV}(SoC)$ (V)) multiplied by the current (I (A)), as stated in Equation (5).

$$\dot{Q}_{gen} = |V - V_{OCV}(SoC)|I \tag{5}$$

For this research, where we are seeking to determine the cell heat capacity, the voltage and current are obtained from experiments. In future, if the model is to be made truly predictive, the thermal model demonstrated here would need to be combined with a model to predict the voltage and current for a given load profile and these models are widely available, for example equivalent circuit models [23,24].

3. Experimental setup

An advantage of the thermal model described in this paper is that the equipment required to characterise the cells and demonstrate the model are common and found in many laboratories. The required equipment is:

- Equipment capable of charging and discharging a cell and recording the voltage and current;
- At least two temperature sensors, one for the cell surface and one for recording ambient temperature;
- Equipment capable of increasing the heat transfer from the cell to the ambient, such as fans.

For the experiments in this paper, a Maccor Model 4200 with type T thermocouples is used to charge and discharge the cells and to record the cell voltage, current and temperature. Two computer fans are used to provide air flow and promote heat transfer from the cell to the ambient and one of the cells under test is illustrated in Fig. 2a. In this study, nine thermocouples for the cylindrical cells and ten thermocouples for the pouch and prismatic cells are placed on the cell surfaces, in the locations shown in Fig. 2b, and the average of the thermocouples is used as the measure of the surface temperature. Surface temperature variations and varying the number of thermocouples for the experiment are discussed in Section 8.

Details of the four lithium-ion cells tested are given in Table 1. Exact details of the chemistries of the cells are not known however three of the cells use Nickel Manganese Cobalt (NMC) as the cathode material and one of the cells uses Iron Phosphate (LFP) as the cathode material. The three NMC cells all have significantly different geometries, with one being a cylindrical 26650 cell, one being a pouch cell and one being a prismatic cell. While the LFP cell is also a cylindrical 26650 cell. None of the datasheets provided by the manufacturers state a value for the heat capacity of the cells and, when contacted, none of the manufacturers were able to provide data on the heat capacities of the cells.

At high currents the connection of the current carrying wires to the cell is important as a poor connection will result in additional ohmic heat generation at the point of connection. There are commonly three types of cell connections: mechanical connectors, welding or soldering. For the experiments conducted in this paper, soldering is used for the cylindrical cells. Of the three methods, soldering should give the best connection however the heat during soldering may reduce the lifetime of the cell. The lifetime of the cell is not a focus of this study and, after soldering, charge and discharge tests are conducted on each of the cells to ensure the voltage and capacity plots are not affected by the soldering. For the pouch cells the tabs are clamped with the current carrying wire in between copper connectors and for the prismatic cells the current carrying wire is bolted to the cell tab.

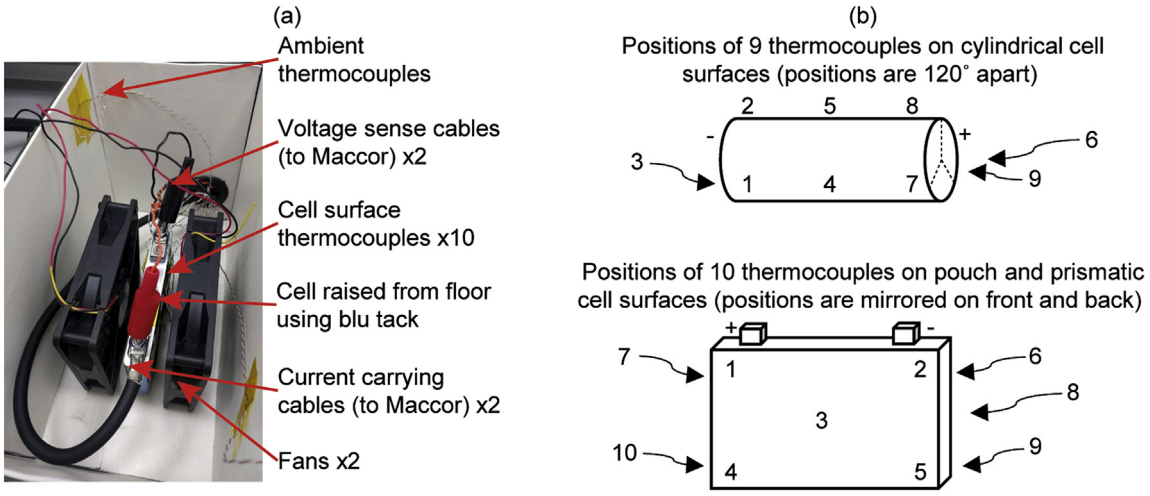

Fig. 2. Picture of cell testing setup for the NMC prismatic cell (left) and thermocouple placement on cell surfaces (right).

4. Determination of parameters

In this section the heat capacity, the internal thermal resistance and the external thermal resistance, detailed in Equation (3), are determined. The heat capacity and internal thermal resistance are specific to each cell, once they have been determined the cell can be tested in different scenarios and only the external thermal resistance changes. The external thermal resistance is determined in Section 4.1 and the heat capacity and internal thermal resistance determined in Section 4.2, where examples are shown for the NMC 26650 cell.

4.1. External thermal resistance

To determine the external thermal resistance a similar method to that described in [22] is used. The cell is taken to 50% state of charge by discharging the cell to the lower cut off voltage and then charging the cell until half the capacity has been added to the cell. The cell is then left overnight and the voltage recorded the following day is taken as the open circuit voltage for the test. The cell is then discharged a small amount, less than 5% rated capacity, at the maximum discharge rate allowed by the manufacturer from Table 1. The cell is then charged by the same amount of capacity as just removed at the manufacturers maximum charge rate. This discharge/charge cycle is then repeated until the surface temperature remains constant, dT_s/dt then equals zero and Equation (3) then simplifies to Equation (6), where $\dot{Q}_{gen}$ is defined by Equation (5).

$$0 = \dot{Q}_{gen} R_{out} + T_a - T_s \tag{6}$$

For the lithium-ion NMC 26650 cell the results are shown in Fig. 3. The cell is discharged at its maximum discharge current from the datasheet of 15 A until 0.021 Ah are removed, taking 5 s, the cell is then charged at its maximum charge current of 5 A until 0.021 Ah are added, taking 15 s, as shown in Fig. 3a. The open circuit voltage (V_{OCV}) is recorded before the test as 3.726 V. Fig. 3b and c show the heat generated, which is calculated using Equation (5), and Fig. 3d shows the cell surface and ambient temperatures during the experiment. As is clear from Fig. 3d, after 1 h the surface temperature has stabilised and is no longer increasing and the test then continues in a stable fashion for a further hour. To obtain the variables in Equation (6) average values over the final 30 min of the test are used (*Section_fin* in Fig. 3d), the average heat generation is 1.62 W, the average ambient temperature (T_{a_fin}) is 23.7 °C and the average surface temperature (T_{s_fin}) is 34.6 °C. The external thermal resistance is therefore calculated using Equation (6) as 6.7 K W^{-1}.

4.2. Specific heat capacity and internal thermal resistance

To determine the remaining parameters, the same experiment as in Section 4.1 is used, however only the period when the surface temperature is increasing is considered. The time period considered runs from 0 min until the time when the surface temperature is 95% of the way to the final average surface temperature (*Section_init* in Fig. 3d). For the case demonstrated in Section 4.1, 95% of the way between the final ambient and surface temperatures (23.7 °C and 34.6 °C respectively) is 34.1 °C, which occurs after 1950 s. Least squares regression of Equation (4) is used to fit the surface temperature, with the pre-established value for R_{out}, to find a value for $C_p(R_{in} + R_{out})$, this is the denominator of Equation (4). When performing the least squares regression the ambient temperature in the initial section (T_{a_init}) is used. This is demonstrated for the NMC 26650 cell in Fig. 4, where the time

Table 1
Details of the cells tested.

	NMC 26650	LFP 26650	NMC Pouch	NMC Prismatic
Manufacturer	AAPortable Power	A123 Systems	AAPortable Power	GS Yuasa
Geometry	Cylindrical 26650	Cylindrical 26650	Pouch	Prismatic
Dimensions	Ø26 mm × 65 mm	Ø26 mm × 65 mm	11 mm × 60 mm × 162 mm	16 mm × 79 mm × 112 mm
Name	INR-26650-5000	ANR26650M1-B	10059156-5C	LIM5H
Nominal Voltage (V)	3.6	3.3	3.7	3.6
Capacity (Ah)	5	2.5	10	5
Mass (g)	96	76	198	276
Energy density (Wh kg^{-1})	190	110	190	65
Charge cut-off voltage (V)	4.2	3.6	4.2	4.2
Discharge cut-off voltage (V)	2.75	2.0	2.75	2.4
Maximum continuous charge current (A)	5	10	10	50
Maximum continuous discharge current (A)	15	70	40	50

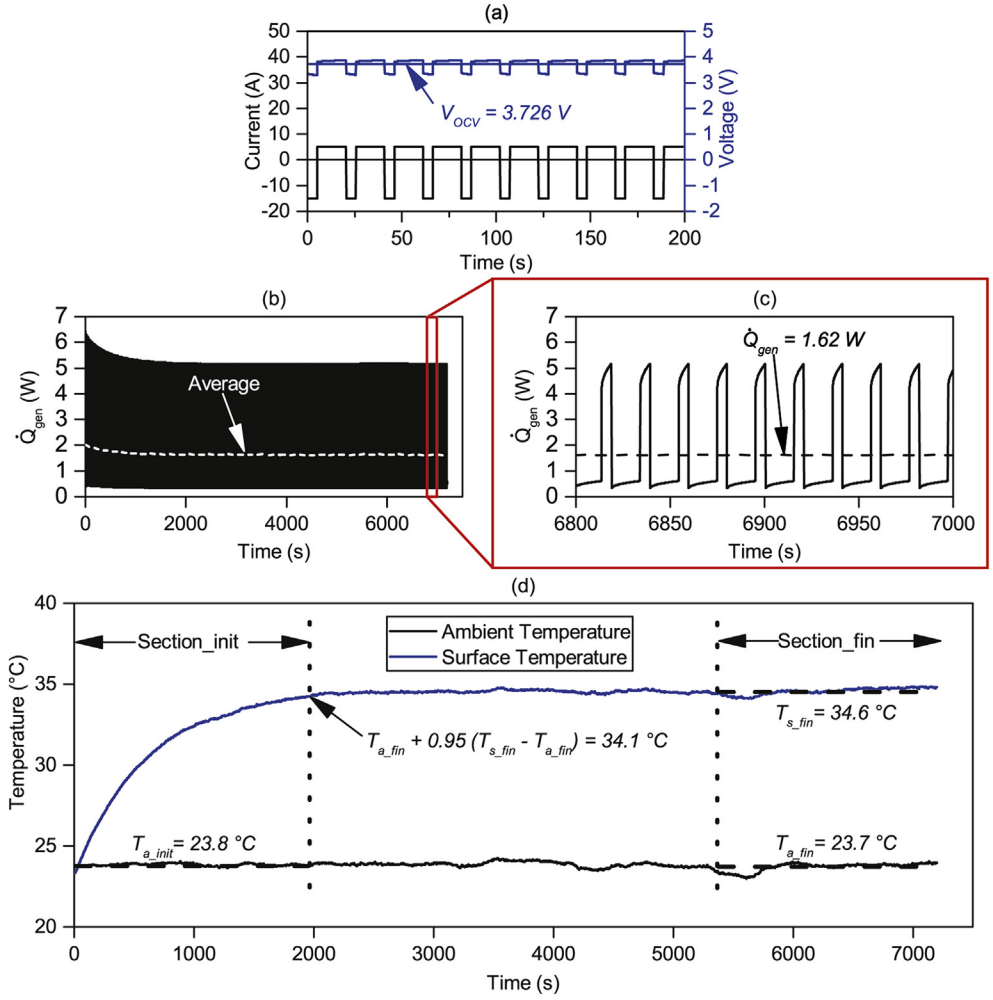

Fig. 3. NMC 26650 cell: current applied to cell and voltage response for first 200 s (top), heat generation calculated using Equation (5) (middle), temperature response of cell (bottom).

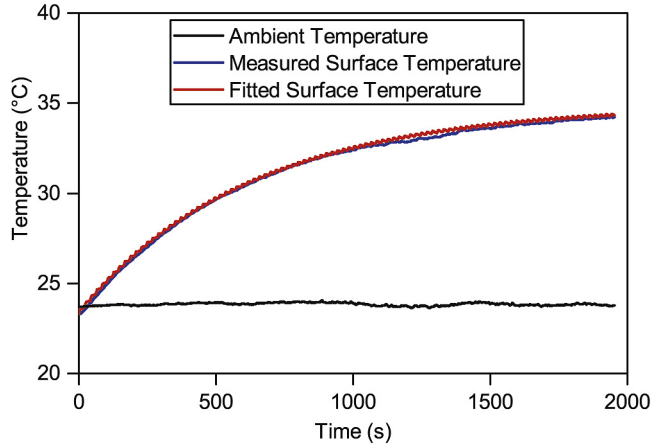

Fig. 4. NMC 26650 cell: *Section_init* from Fig. 3, where the fitted temperature curve has been created using Equation (4) and a value of $C_p(R_{in} + R_{out})$ of 750 s determined using least squares regression.

step used is 0.1 s and the value for $C_p(R_{in} + R_{out})$ found as 750 s.

A fan is then set up to blow air over the cell thereby increasing the heat transfer from the cell to ambient and lowering the external thermal resistance. The heat capacity and internal thermal resistance however remain the same. The same experiment from Section 4.1 is then conducted to find the value of the external thermal resistance with the fan.

The least squares regression described above is also repeated to find a value for $C_p(R_{in} + R_{out})$ with the fan. Two simultaneous equations can then be produced and solved to find values for the heat capacity and internal thermal resistance. This is demonstrated in Equation (7) for the NMC 26650 cell. The values of R_{out} and $C_p(R_{in} + R_{out})$ with the fan for the NMC 26650 cell are 1.8 K W^{-1} and 290 s respectively.

$$C_p(R_{in} + 6.7) = 750 \ \ (No\ fan)$$
$$C_p(R_{in} + 1.8) = 290 \ \ (Fan)$$
$$C_p = 94\ J\ K^{-1},\ \ R_{in} = 1.3\ K\ W^{-1} \tag{7}$$

The specific heat capacity (c_p ($J\ kg^{-1}\ K^{-1}$)) is found by dividing the heat capacity by the mass of the cell, listed in Table 1. For the NMC 26650 cell the specific heat capacity is found to be 980 J kg^{-1} K^{-1}.

5. Calorimetry experiments

To verify the specific heat capacity results, experiments are performed in a calorimeter, in this instance the Thermal Hazards Technology ARC EV + calorimeter, using a method suggested by the manufacturer. The method involves grouping multiple cells together using aluminium tape, so that a Kapton heater can be placed in between the cells such that all the heat generated from the heater is absorbed by the cells. A thermocouple is attached to the outside of the cells with aluminium tape to measure the temperature rise at the surface of the cells. Two cells are used for the pouch and prismatic cell calorimetry and three cells for the cylindrical 26650 cell calorimetry. The cells are

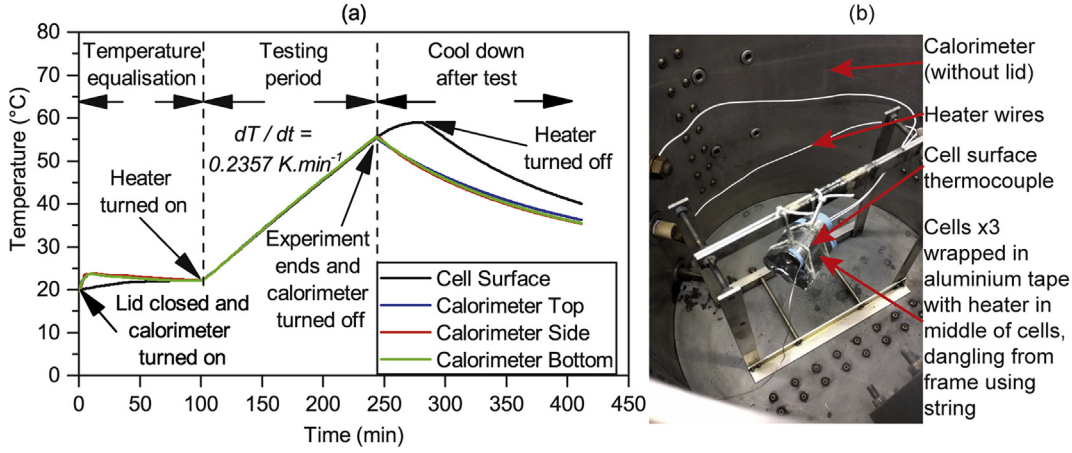

Fig. 5. Calorimeter experiment for NMC 26650 cell.

each weighed individually and then again when combined together with the heater and aluminium tape. The cells with the heater are then hung from string in the calorimeter, such that the cells are suspended away from the calorimeter walls to prevent direct heating and to avoid any possible heat loss by conduction as any heat conduction through the string would be negligible, shown in Fig. 5b.

The calorimeter is then sealed and the temperature is set to 25 °C and left to rest to allow the cells to equilibrate with the calorimeter, during the 'Temperature equalisation' period between 0 and 100 min in Fig. 5a. The calorimeter is then put in exotherm mode in which near adiabatic conditions are created within the calorimeter, by the temperature being set to follow the cell surface temperature. The power to the heater is then switched on using a constant voltage power supply. A Kapton heat mat is used because the resistance of the heat mat does not change with temperature so the power supplied to the heater is constant throughout the test. The region of adiabatic temperature rise can be seen during the 'Testing period' between 100 and 250 min in Fig. 5a. Once the temperature of the cells reaches 55 °C the experiment is over and the calorimeter stops tracking the cell temperature, the heater is switched off to conclude the experiment.

The heat capacity of the entire sample placed in the calorimeter (C_{pTOT} $(J\ K^{-1})$) is found using Equation (8). The rate of change of temperature with time (dT/dt $(K\ s^{-1})$) is taken from Fig. 5a, the slope of the adiabatic temperature rise, and the power (P (W)) is calculated as the voltage across the heater multiplied by the current through the heater (for these experiments being 11.97 V and 0.09563 A respectively). The specific heat capacity of the cells is then found by removing the heat capacity of the aluminium tape from the sample by weight using Equation (9). The equation uses total sample mass (m_{TOT} (kg)) the individual cell mass (m_{cell} (kg)), the number of cells (n_{cells}) and the specific heat capacity of aluminium (c_{pAl} $(J\ kg^{-1}\ K^{-1})$), for the NMC 26650 cells these values are 0.298 kg, 0.096 kg, 3 cells and 913 J kg^{-1} K^{-1} respectively. The specific heat capacity of the NMC 26650 cell is therefore calculated from the calorimetry as 980 J kg^{-1} K^{-1}.

$$P = C_{pTOT}\frac{dT}{dt} \tag{8}$$

$$C_{pTOT} = (m_{TOT} - m_{cell}n_{cells})c_{pAl} + m_{cell}n_{cells}c_p \tag{9}$$

To determine the accuracy of the calorimeter experiment in determining heat capacity values, a test run is conducted on a sample of three rods of Aluminium, with the same geometry as a 26650 cell. A value for the specific heat capacity of 939 J kg^{-1} K^{-1} is obtained from the experiments, which is within 3% of the value quoted in data books for aluminium of 913 J kg^{-1} K^{-1}.

6. Results

The experiments using the new method are conducted three times without the fans and three times with the fans. The results for the specific heat capacities, internal resistances and external resistances are given in the following sections. The specific heat capacity and internal thermal resistance results of the cells are important, the results obtained using the method described in this paper could be used in a model of a battery module or pack. The external thermal resistance results are less important because they are specific to the testing conditions described in this paper. In a thermal model of a battery module or pack the specific heat capacity and internal thermal resistance would stay the same while the heat transfer away from the cell will depend on the cell location in the module or pack. The external thermal results are presented for reference and are also used in the validation of the model in section 7.2.

6.1. Specific heat capacity and internal thermal resistance values

The results for the specific heat capacity and internal thermal resistance of the cells are given in Table 2 and a graphical comparison of the specific heat capacities illustrated in Fig. 6. Results are given for both the new method and the experiments conducted in the calorimeter.

For each cell, three experiments are conducted without the fans and three experiments conducted with the fans, giving a total of nine calculated specific heat capacities for each cell. In Fig. 6 the error bars show the highest and lowest specific heat capacities calculated using the new method. The reason for differences between the tests is the ambient temperature variations, all experiments except the NMC prismatic cells had ambient temperature changes of less than 1 °C in the *section_init* and *section_fin* stages seen in Fig. 3d. For the NMC prismatic cell, 50 A is the current continuously applied to the cell and as such the ambient surroundings heated up more. For these experiments the

Table 2
Results for specific heat capacities, the values shown for the new method are the mean values obtained, and the internal thermal resistance results.

	NMC 26650	LFP 26650	NMC Pouch	NMC Prismatic
c_p – New method (J kg^{-1} K^{-1})	978	1169	1182	1012
c_p – Calorimetry (J kg^{-1} K^{-1})	981	1127	1138	1037
Difference (%)	- 0.3	+3.8	+3.9	- 2.3
R_{in} (K W^{-1})	1.4	1.4	0.26	0.42

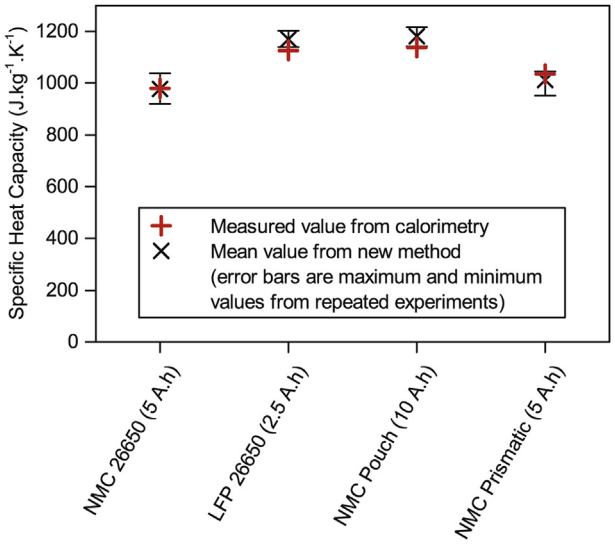

Fig. 6. Graphical comparison of results obtained using the new method and results obtained using calorimetry.

ambient change is kept to under 2.5 °C. The largest percentage difference between the specific heat capacity found for the repeated experiments using the new method and the calorimeter value is less than 10% in all cases, with the worst case differences for the NMC 26650, LFP 26650, NMC Pouch and NMC prismatic cells being 6.2%, 6.6%, 6.9% and 8.1% respectively.

The results obtained using the new method evidence good correlation with the results obtained using the calorimeter. The calorimeter results show the LFP 26650 and NMC Pouch cells have higher specific heat capacities than the NMC 26650 and NMC Prismatic cells and the new method correctly predicts this. The order, from the NMC 26650 with the lowest to the NMC Pouch cell with the highest specific heat capacity, is also correctly predicted by the new method.

The internal resistance results represent the thermal resistance, mainly due to conduction, from the centre of the cell to the cell surface. To consider the internal thermal resistance results the ratio of distance to the cell surface area can be examined. The distance is taken from the centre of the cell to the cell surface, for the cylindrical cells this is taken as the radius and for the pouch and prismatic cells this is taken as half the thickness. This ratio is $2.0\,m^{-1}$, $0.23\,m^{-1}$ and $0.34\,m^{-1}$ for the cylindrical, pouch and prismatic cells respectively. To convert this ratio to a thermal resistance it needs to be divided by the thermal conductivity. For this initial validation it is assumed that the thermal conductivity is similar for all cells, it can then be seen that the results for the internal thermal resistance from Table 2 follow the trend of this simple calculation well, i.e. the cylindrical cells have an internal thermal resistance around an order of magnitude above the pouch and prismatic cells. This simple calculation only accounts for heat conducted through the cell in one direction and as described the thermal conductivity through the cell will be different in different directions and different between the cells, nevertheless it is an intermediate validation of the result.

6.2. External thermal resistance

The external thermal resistance results represent the thermal resistance, mainly due to convection, from the cell surface to the ambient. The external thermal resistance due to convection is related to the size of the cell but also dependent on the geometry, i.e. cylinder or cuboid. The results for the external resistance can be seen in Table 3. The results are very similar for both cylindrical 26650 cells, which is logical as they have exactly the same geometry. The results are also very similar for the pouch and prismatic cells, which is also logical as their geometry is similar and they have similar surface areas. The external thermal resistance is lower for the pouch and prismatic cells than the cylindrical 26650 cells because of the larger surface area, which makes heat transfer from the cell surface to the ambient easier. In all cases it can also be seen that the thermal resistances decrease with the use of fans as heat transfer is being increased from the cell surface to the ambient.

Table 3
External thermal resistance results.

	NMC 26650	LFP 26650	NMC Pouch	NMC Prismatic
R_{out} – no fans ($K\,W^{-1}$)	6.7	6.6	3.1	3.1
R_{out} – fans ($K\,W^{-1}$)	1.8	1.6	0.70	0.73

7. Validation of model

In this section it is demonstrated how the cell thermal parameters obtained can be used to effectively model the surface temperature of the cells under various scenarios. Modelling the cell temperature during operation is often required to ensure the cell is kept within the required temperature limits and also to calculate the cooling power required for application thermal management.

7.1. Open circuit voltage

Initially a plot of open circuit voltage versus state of charge for each of the cells is obtained, where this is defined as the input $V_{OCV}(SoC)$ in Equation (5). The open circuit voltage is found by charging the cell by 5% of the rated capacity and then allowing the cell to rest for 15 min and recording the final voltage, this is repeated for all states of charge 5%, 10%, …, 100%. This test is then repeated during discharge and so a plot of voltage after a 15 min rest during charge and discharge for a range of state of charges is obtained. The open circuit voltage is then assumed to be the average value between the charge and discharge voltage values, as demonstrated in Fig. 7a for the NMC 26650 cell. Before each charge and discharge test the cell is left overnight, it is therefore assumed that the values at the start of each charge and discharge test are the open circuit voltage at 0% and 100% states of charge. The open circuit voltage versus state of charge for each cell can be seen in Fig. 7b.

7.2. Demonstration of model

To demonstrate the effective behaviour of the authors' cell model the cells are tested under charge and discharge at different C-rates, using the constant current method for both charge and discharge between the cell cut off voltages seen in Table 1. The cells are charged at 1C and then discharged at 3C, 2C and 1C with a 10 min rest between each step with the results being shown in Fig. 8. All graphs in Fig. 8 have been created using the values for c_p and R_{in} given in Table 2 and modelled using Equation (4). The state of charge at each time is calculated using coulomb counting. The tests seen in Fig. 8a and b are conducted in the same conditions as the experiments to determine the heat capacity and so the values of R_{out} seen in Table 3 are used. The test shown in Fig. 8c is conducted in a freezer meaning the ambient temperature is lowered however the value of R_{out} is also taken from Table 3 as the heat transfer from the cell to ambient is still the same as previous experiments because the cell is simply resting on blu tack on the floor of the freezer. The heat transfer from the cell to the ambient has been changed for Fig. 8d by wrapping the cell in 25 mm Armaflex insulation. A value of $15\,K\,W^{-1}$ is obtained for R_{out} for the cell wrapped in insulation using the same methodology described in Section 4.1.

It is clear from the results the modelled temperature closely matches that of the temperature obtained during the thermal experiments hence providing further evidence of the authors' heat capacity modelling

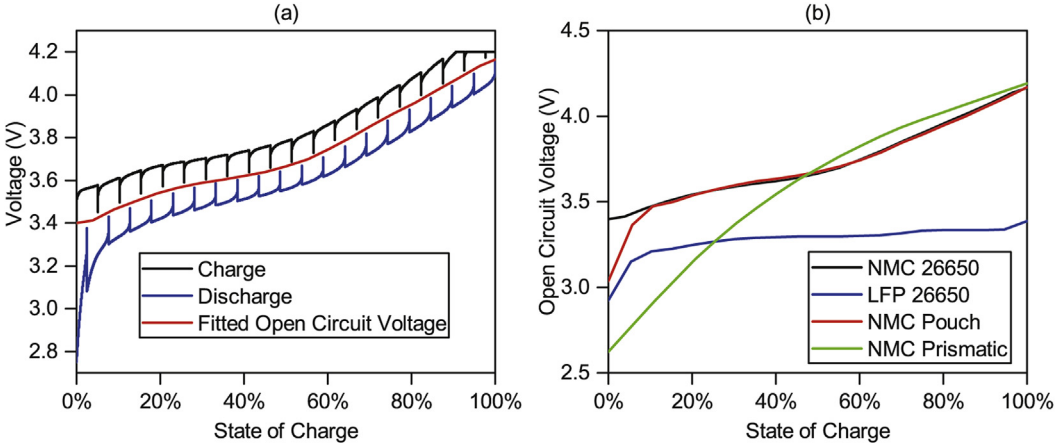

Fig. 7. Experimental results to determine the open circuit voltage for the NMC 26650 cell (left) and open circuit voltage for all cells (right).

methodology and the accuracy of the approach described in this paper. For the conditions tested the maximum error is 3.1 °C after the 3C discharge of the NMC 26650 in the freezer. Differences may arise as a result of variations in temperature and heat transfer in the cell or as a result of other modes of heat generation or consumption not included in this model.

It can be seen that even though only one mode of heat generation is considered the model accurately predicts the surface temperature. This is because the examples given are at high rates, over 1C, and so the ohmic heating generation is the dominant mode of heat generation. If the temperature response at lower rates is required it is likely additional modes of heat generation would need to be considered.

Fig. 8d is perhaps the most interesting result as it shows that once the methodology described in this paper has been utilised to obtain the specific heat capacity and internal thermal resistance of the cells, the values obtained can be used to model the cell under significantly different conditions. For this case the cell has been wrapped in insulation however the cell could also be placed in a model of a battery module or pack. If the cell is modelled in a battery module, finite element modelling would likely be required as the heat transfer to and from the cell becomes more complicated due to heat generated by nearby cells. The thermal model of the module or pack could however use the specific heat capacity and internal resistance of the cells determined using the method described in this paper.

7.3. Cycling efficiency and heat

The model used in this paper assumes all the heat generation is as a result of ohmic heat generation, therefore it should be possible to relate the energy lost during charging and discharging to the heat energy leaving the cell calculated using the model in this paper. The energy lost during charge and discharge (E_{loss}) is calculated as per Equation (10), netting the energy supplied to charge the cell (E_{charge}) with the energy delivered whilst discharging the cell ($E_{discharge}$), both of which are recorded by the battery analyser.

$$E_{loss} = E_{charge} - E_{discharge} \tag{10}$$

The heating power calculated using the model in this paper is equal to the rate heat flows away from the cell, which was defined as the right hand side of Equation (2). To calculate the heat energy leaving the cell this power is integrated over the required period as per Equation (11).

$$E_{heat} = \int \frac{1}{R_{out}}(T_s(t) - T_a)dt \tag{11}$$

To test the hypothesis, the cycles shown in Fig. 8a are used, with an initial 1C charge also included to ensure three charge and three discharge steps are used. The test started and finished with the cell at ambient temperature after a rest period. Using Equation (10) and Equation (11), E_{loss} and E_{heat} are calculated as 23,800 J and 23,000 J respectively. This good match means that Equation (11) could be used to estimate the energy to be removed by a battery cooling system if the cell was in a battery module or pack. The calculation is only an estimate as, if a cooling system kept the cell temperature lower or higher, the internal cell resistance would change, thereby changing the heat generation and cooling required.

8. Temperature variations analysis

The model described in this paper does not take into account variations of temperature across the surface of the cells. The close match of the results obtained using the authors' new method and the results obtained from separate calorimeter tests indicate that not taking into account surface temperature variations is a reasonable assumption. For these experiments the maximum variation in temperature across the surface of the cells is observed to be 2.7 °C, when a surface thermocouple at the centre of the NMC Prismatic cell is hotter than a thermocouple near the corner of the cell.

To examine the effect of surface temperature variations further, the same experiments to determine the specific heat capacity are conducted however with only one thermocouple (thermocouple 5) for the cylindrical cells and two thermocouples (thermocouples 3 and 8) for the pouch and prismatic cells. The results for specific heat capacity are 1.8%, 2.9%, 2.6% and 3.6% different to those obtained from the calorimeter experiments for the NMC 26650, LFP 26650, NMC Pouch and NMC Prismatic respectively. This indicates that in future the method could be conducted with only one or two surface thermocouples and one ambient thermocouple.

The cell surface temperature variations are greater during the charging and discharging of the cells at various C-rates as shown in Fig. 8. In these experiments the NMC 26650 cell in the freezer had a maximum surface temperature variation of 6.7 °C, when a surface thermocouple at the centre of cell was reading 38.4 °C and a thermocouple near the negative electrode reading 31.7 °C. Although, the maximum temperature difference across the surface is 6.7 °C, when average values are used it can be seen in Fig. 8c the maximum difference between the modelled and average surface temperature is less than 2 °C.

Not taking into account surface variations is a limitation of the model described in this paper. However, other thermal models that do take into account temperature variations across cell surfaces often still only use a single value for the specific heat capacity for the entire cell [25,26]. This means that even if a more complicated thermal model involving surface temperature variations is required, the method to determine the specific heat capacity described in this paper is still

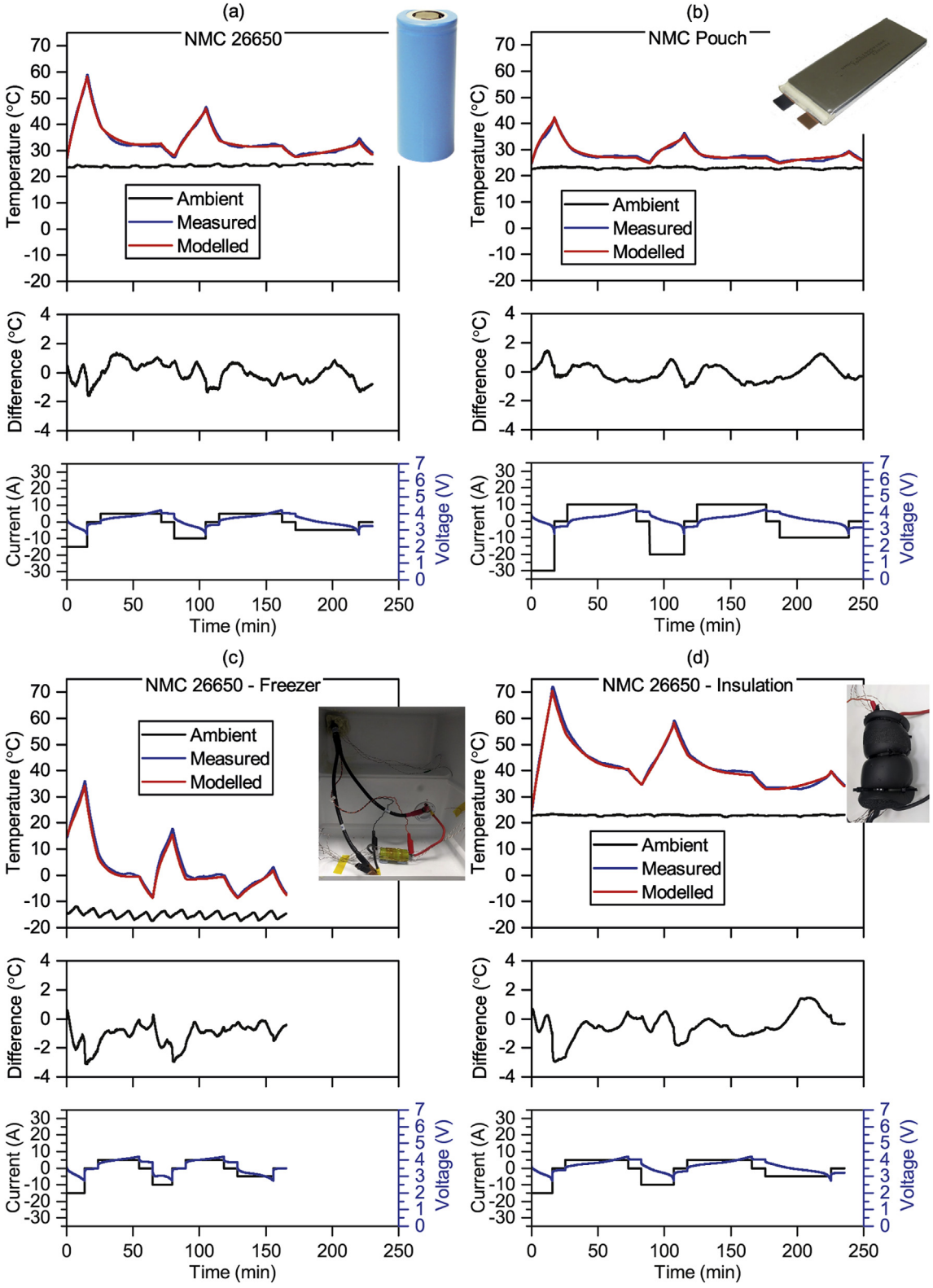

Fig. 8. Modelled versus measured temperatures for the cells tested.

useful.

9. Conclusions

The archival value of this paper is a new method to determine the specific heat capacity of any lithium-ion cell, the specific heat capacity is vital for the thermal modelling of batteries and not supplied on datasheets or given by manufacturers. The equipment required is common to most battery laboratories and no expensive environment chambers or calorimeters are required. The method has been validated for cylindrical, pouch and prismatic cell types, with capacities between 2.5 Ah and 10 Ah, by comparing the specific heat capacity results obtained

from the model to results obtained using a calorimeter. For the cells tested the maximum error in determined specific heat capacity is 8.1% however when the mean values are used, the maximum error is reduced to 3.9%. Once the method described in this paper has been conducted, the specific heat capacity obtained can then be used in thermal modelling of battery modules or battery packs.

It has also been shown how, once the method described in this paper has been used to obtain the thermal parameters, these thermal parameters can be used to model the surface temperature of the cells at C-rates over 1C. For modelling lower current rates or for more detail regarding the temperature variation in and on the surface of the cell, the model may not be sufficient. However, for many cases, this simple model may be sufficient and even if a more complicated thermal model is required, the method to determine the cell heat capacity and internal thermal resistance will be useful inputs for these models.

Acknowledgements

This research was supported by funding from the EPSRC through two grants “EPSRC Centre for Doctoral Training in Energy Storage and its Applications” [grant number EP/L016818/1] and “ELEVATE (ELEctrochemical Vehicle Advanced TEchnology)” [grant number EP/M009394/1].

References

[1] G. Xia, L. Cao, G. Bi, A review on battery thermal management in electric vehicle application, J. Power Sources 367 (2017) 90–105, http://dx.doi.org/10.1016/j.jpowsour.2017.09.046.

[2] S. Abada, G. Marlair, A. Lecocq, M. Petit, V. Sauvant-Moynot, F. Huet, Safety focused modeling of lithium-ion batteries: a review, J. Power Sources 306 (2016) 178–192, http://dx.doi.org/10.1016/j.jpowsour.2015.11.100.

[3] M. Keyser, A. Pesaran, Q. Li, S. Santhanagopalan, K. Smith, E. Wood, et al., Enabling fast charging – battery thermal considerations, J. Power Sources 367 (2017) 228–236, http://dx.doi.org/10.1016/j.jpowsour.2017.07.009.

[4] G.S. Yuasa, Blue Energy Lithium-ion Batteries to be Used in Honda's New Clarity Fuel Cell Vehicle, (2016) Available: https://www.yuasa.co.uk/2016/05/2629/ , Accessed date: 17 April 2018.

[5] K. Onda, T. Ohshima, M. Nakayama, K. Fukuda, T. Araki, Thermal behavior of small lithium-ion battery during rapid charge and discharge cycles, J. Power Sources 158 (2006) 535–542, http://dx.doi.org/10.1016/j.jpowsour.2005.08.049.

[6] Y. Kim, S. Mohan, J.B. Siegel, A.G. Stefanopoulou, Y. Ding, The estimation of temperature distribution in cylindrical battery cells under unknown cooling conditions, IEEE Trans. Contr. Syst. Technol. 22 (2014) 2277–2286, http://dx.doi.org/10.1109/tcst.2014.2309492.

[7] J. Jaguemont, N. Omar, F. Martel, P. Van den Bossche, J. Van Mierlo, Streamline three-dimensional thermal model of a lithium titanate pouch cell battery in extreme temperature conditions with module simulation, J. Power Sources 367 (2017) 24–33, http://dx.doi.org/10.1016/j.jpowsour.2017.09.028.

[8] T. Grandjean, A. Barai, E. Hosseinzadeh, Y. Guo, A. McGordon, J. Marco, Large format lithium ion pouch cell full thermal characterisation for improved electric vehicle thermal management, J. Power Sources 359 (2017) 215–225, http://dx.doi.org/10.1016/j.jpowsour.2017.05.016.

[9] Z. Wang, J. Ma, L. Zhang, Finite element thermal model and simulation for a cylindrical Li-Ion battery, IEEE Access 5 (2017) 15372–15379, http://dx.doi.org/10.1109/ACCESS.2017.2723436.

[10] E. Gümüşsu, Ö Ekici, M. Köksal, 3-D CFD modeling and experimental testing of thermal behavior of a Li-Ion battery, Appl. Therm. Eng. 120 (2017) 484–495, http://dx.doi.org/10.1016/j.applthermaleng.2017.04.017.

[11] X. Lin, H.E. Perez, J.B. Siegel, A.G. Stefanopoulou, Y. Li, R.D. Anderson, et al., Online parameterization of lumped thermal dynamics in cylindrical lithium ion batteries for core temperature estimation and health monitoring, IEEE Trans. Contr. Syst. Technol. 21 (2013) 1745–1755, http://dx.doi.org/10.1109/TCST.2012.2217143.

[12] U.S. Kim, J. Yi, C.B. Shin, T. Han, S. Park, Modelling the thermal behaviour of a lithium-ion battery during charge, J. Power Sources 196 (2011) 5115–5121, http://dx.doi.org/10.1016/j.jpowsour.2011.01.103.

[13] S. Panchal, M. Mathew, R. Fraser, M. Fowler, Electrochemical thermal modeling and experimental measurements of 18650 cylindrical lithium-ion battery during discharge cycle for an EV, Appl. Therm. Eng. 135 (2018) 123–132, http://dx.doi.org/10.1016/j.applthermaleng.2018.02.046.

[14] R. Benger, H. Wenzl, H.-P. Beck, M. Jiang, D. Ohms, G. Schaedlich, Electrochemical and thermal Modelimh of Lithium-ion Cells for Use in HEV or EV Application, in EVS24, Stavanger, Norway, (2009).

[15] N.S. Spinner, R. Mazurick, A. Brandon, S.L. Rose-Pehrsson, S.G. Tuttle, Analytical, numerical and experimental determination of thermophysical properties of commercial 18650 LiCoO2 lithium-ion battery, J. Electrochem. Soc. 162 (2015) A2789–A2795, http://dx.doi.org/10.1149/2.0871514jes.

[16] D. Werner, A. Loges, D.J. Becker, T. Wetzel, Thermal conductivity of Li-ion batteries and their electrode configurations – a novel combination of modelling and experimental approach, J. Power Sources 364 (2017) 72–83, http://dx.doi.org/10.1016/j.jpowsour.2017.07.105.

[17] K. Shah, S.J. Drake, D.A. Wetz, J.K. Ostanek, S.P. Miller, J.M. Heinzel, et al., Modeling of steady-state convective cooling of cylindrical Li-ion cells, J. Power Sources 258 (2014) 374–381, http://dx.doi.org/10.1016/j.jpowsour.2014.01.115.

[18] K.E. Thomas, J. Newman, Thermal modeling of porous insertion electrodes, J. Electrochem. Soc. 150 (2003) A176–A192, http://dx.doi.org/10.1149/1.1531194.

[19] S. Chacko, Y.M. Chung, Thermal modelling of Li-ion polymer battery for electric vehicle drive cycles, J. Power Sources 213 (2012) 296–303, http://dx.doi.org/10.1016/j.jpowsour.2012.04.015.

[20] M. Al-Zareer, I. Dincer, M.A. Rosen, Novel thermal management system using boiling cooling for high-powered lithium-ion battery packs for hybrid electric vehicles, J. Power Sources 363 (2017) 291–303, http://dx.doi.org/10.1016/j.jpowsour.2017.07.067.

[21] J.P. Schmidt, A. Weber, E. Ivers-Tiffée, A novel and precise measuring method for the entropy of lithium-ion cells: ΔS via electrothermal impedance spectroscopy, Electrochim. Acta 137 (2014) 311–319, http://dx.doi.org/10.1016/j.electacta.2014.05.153.

[22] C. Forgez, D. Vinh Do, G. Friedrich, M. Morcrette, C. Delacourt, Thermal modeling of a cylindrical LiFePO4/graphite lithium-ion battery, J. Power Sources 195 (2010) 2961–2968, http://dx.doi.org/10.1016/j.jpowsour.2009.10.105.

[23] T. Hu, B. Zanchi, J. Zhao, Simple analytical method for determining parameters of discharging batteries, IEEE Trans. Energy Convers. 26 (2011) 787–798, http://dx.doi.org/10.1109/TEC.2011.2129594.

[24] C. Liao, H. Li, L. Wang, A dynamic equivalent circuit model of LiFePO4 cathode material for lithium ion batteries on hybrid Electric vehicles, In 2009 IEEE Vehicle Power and Propulsion Conference, Dearborn, MI, USA, 2009, http://dx.doi.org/10.1109/VPPC.2009.5289681.

[25] E. Hosseinzadeh, R. Genieser, D. Worwood, A. Barai, J. Marco, P. Jennings, A systematic approach for electrochemical-thermal modelling of a large format lithium-ion battery for electric vehicle application, J. Power Sources 382 (2018) 77–94, http://dx.doi.org/10.1016/j.jpowsour.2018.02.027.

[26] Z. Rao, Z. Qian, Y. Kuang, Y. Li, Thermal performance of liquid cooling based thermal management system for cylindrical lithium-ion battery module with variable contact surface, Appl. Therm. Eng. 123 (2017) 1514–1522, http://dx.doi.org/10.1016/j.applthermaleng.2017.06.059.